Journal of Applied Physics ARTICLE pubs.aip.org/aip/jap

Spin-dependent recombination affected by post-annealing of organic photovoltaic devices

Cite as: J. Appl. Phys. **135**, 075002 (2024); doi: 10.1063/5.0174969
Submitted: 4 September 2023 · Accepted: 27 December 2023 ·
Published Online: 15 February 2024

Takayuki Suzuki[1,2] and Kazuhiro Marumoto[1,3,a)]

AFFILIATIONS

[1]Division of Materials Science, Institute of Pure and Applied Sciences, University of Tsukuba, Tsukuba, Ibaraki 305-8573, Japan
[2]JEOL Ltd., 3-1-2 Musashino, Akishima, Tokyo 196-8558, Japan
[3]Tsukuba Research Center for Energy Materials Science, University of Tsukuba, Tsukuba, Ibaraki 305-8571, Japan

[a)]**Author to whom correspondence should be addressed:** marumoto@ims.tsukuba.ac.jp

ABSTRACT

Organic photovoltaic devices (OPVs) are attracting attention because of recent rapid enhancement of their power conversion efficiency. For further improvement, optimization of fabrication processes is one useful path to a solution. During OPV fabrication, particularly of the bulk heterojunction active layer, annealing treatments contribute to the device performance. Many studies have examined annealing-related properties. However, further research must clarify how paramagnetic species in the devices play their roles by annealing. Using well-known OPVs, we investigated the relation between spin-dependent recombination (SDR) current and the paramagnetic species, which vary the numbers by post-annealing with active layers consisting of poly(3-hexylthiophene-2,5-diyl) (P3HT) and [6,6]-phenyl-C_{61}-butyric acid methyl ester ($PC_{61}BM$). A simultaneous detection method of electron spin resonance (ESR) and electrically detected magnetic resonance (EDMR), which we originally developed, was applied to OPVs for the first time ever reported. Results show that $PC_{61}BM$ anion radicals generated by post-annealing of P3HT:$PC_{61}BM$ OPVs with a lithium fluoride (LiF)/aluminum (Al) electrode do not contribute to the SDR current at the interface and that P3HT cation radicals enhance the SDR current. By contrast, devices with an Al electrode without LiF decrease the total SDR current, although the quantities of cation radical molecules do not vary. This finding suggests that changes of the hole blocking layer in the devices caused by the annealing treatment affect the size of capture cross sections of P3HT cation radicals. Our new method of quantitative observation of the EDMR changes through the ESR signals is expected to be useful for investigating the capture cross sections in OPVs.

I. INTRODUCTION

Since Tang invented organic photovoltaic devices (OPVs),[1] they have been studied very intensively[2] because they are expected to have superior flexibility, harvesting ability of environmental energy, and potential for low-cost processing. Recently, the power conversion efficiency (PCE) of the devices has been enhanced rapidly by the combination of several functional light active materials.[3–5] Nevertheless, several persistent issues are related to degradation and the stability of the devices for commercialization.

The improvement of device fabrication processes and treatments is extremely important. It can enhance performance considerably. Above all, annealing treatments are frequently used. They are regarded as efficient means to improve the performance of OPVs, including a bulk heterojunction (BHJ) as an active layer.[6–10] Moreover, inserting an intermediate layer for the aluminum (Al) electrode, which can serve as an electron transfer layer (ETL) or a hole blocking layer (HBL), contributes higher total performance.[11,12] A particularly interesting material for use as an HBL is lithium fluoride (LiF). Originally, LiF was adopted for lowering the electrode work function of organic light emitting diodes (OLEDs).[13–15] It improved the performance efficiently. Subsequently, this electrode structure has been applied for OPVs and has demonstrated the effect.[16,17] However, contrary to the well-known annealing effect, earlier reports have described that post-annealing of an OPV with an LiF/Al electrode worsened the performance.[18] One study[18] using secondary ion mass spectrometry (SIMS) profiling measurements has clarified that lithium diffuses into the active organic layer by post-annealing treatment, although an LiF layer is stably maintained before annealing.

Using electron spin resonance (ESR) spectroscopy, Liu *et al.* found that post-annealing enhances the chemical reaction of lithium and [6,6]-phenyl-C_{61}-butyric acid methyl ester ($PC_{61}BM$) and forms $PC_{61}BM$ anion radicals.[19,20]

Actually, ESR spectroscopy is a particularly useful method for selective detection of polarons that have properties of both charges as carriers in organic semiconductor materials and spins. However, using only the ESR method, it remains indistinguishable whether observed polarons contribute to the recombination current at an interface between an Al electrode and an active layer or not. Electrically detected magnetic resonance (EDMR), which is magnetic resonance spectroscopy that is different from ESR, is used for examination of semiconductor devices. Using EDMR, spin-dependent recombination (SDR) current can be detected directly. Therefore, it presents the benefit that target paramagnetic species is distinguished according to whether it contributes to the recombination current directly or not. If ESR and EDMR spectra of devices under operation could be obtained simultaneously, then the relation between paramagnetic species and the recombination current could be observed in real time. Moreover, by clarifying a proportional relation of signal intensities between ESR and EDMR, evaluating the variety of EDMR intensities precisely can be expected by correcting the Q_L-values and B_1 intensities of a microwave cavity because of variations in quality from lot to lot. Here, the Q_L-value denotes a loaded Q value of a cavity resonator. Also, B_1 is the strength of a microwave magnetic field component perpendicular to the static magnetic field in the cavity resonator.

This study explores the correlation between paramagnetic species and the variation of SDR current by post-annealing treatment using an originally developed ESR–EDMR simultaneous detection method[21] applied for the first time to OPVs. By fabricating BHJ-OPVs with an LiF/Al electrode or an Al electrode, radical species that affect SDR current by post-annealing treatment are studied using ESR together with EDMR. Comparing the ESR spectra to those obtained using EDMR reveals that the SDR current through cation radicals is increased because of enlargement of the hole capture cross section by destroying the interface at an LiF/Al electrode. At the same time, it can be clarified that anion radicals observed based on ESR measurements do not contribute directly to the SDR current at the interface. By contrast, a device with an Al electrode develops an effective HBL by post-annealing and suppresses the total SDR current because of the decreased contact area of cation radicals to the Al electrode. Because the observed SDR current flows in the opposite direction of a light-induced one when light irradiates the devices, the SDR current inhibits the short-circuit current (J_{SC}) and is expected to give a loss to the open-circuit voltage (V_{OC}) of the devices, which can be a useful phenomenon to control the long-term stability of the devices.

II. EXPERIMENTAL

For this study, as presented in Fig. 1(a), device A with an LiF/Al electrode and device B with an Al electrode were fabricated to investigate the relation between electrode structures and post-annealing treatment. Devices of two kinds were fabricated in the following way. Indium tin oxide (ITO) coated quartz substrates (3×20 mm) were cleaned ultrasonically in acetone, isopropyl alcohol, and purified water each for 5 min; their total cleansings were two times. After drying the substrates by flushing a dried N_2 gas, a poly(3,4-ethylenedioxythiophene):poly(styrenesulfonate) (PEDOT:PSS) solution was spin coated at 4000 rpm on the substrate. The electrode region was then wiped using acetone. Subsequently, the substrates were annealed at 110 °C for 10 min on a hot plate. Next, the substrates were moved into a nitrogen-filled glovebox. After being annealed at 110 °C for 10 min on a hot plate in a glovebox, an *o*-dichlorobenzene solution of poly (3-hexylthiophene-2,5-diyl) (P3HT):[6,6]-phenyl-C_{61}-butyric acid methyl ester ($PC_{61}BM$), with concentration of 3.0 wt%, was spin coated onto the PEDOT:PSS layer at 600 rpm. After spin coating, the substrates were heated at 40 °C for 20 min on the hot plate to

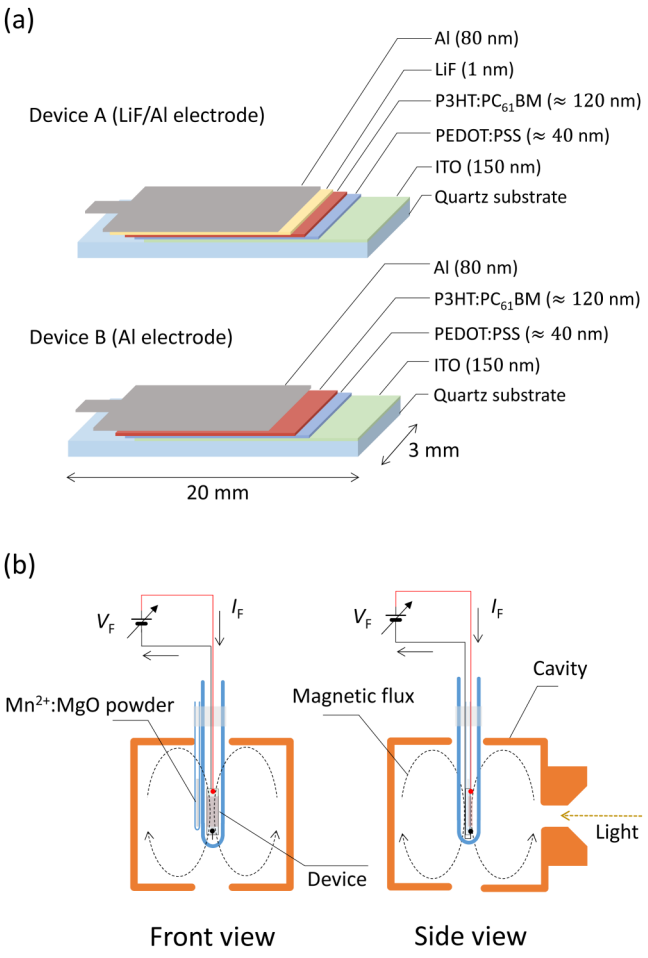

FIG. 1. Fabricated devices and the device setup for simultaneous measurements of ESR and EDMR. (a) Structures of two OPVs. (b) Sketch drawing of the device setting to a cavity resonator for ESR–EDMR measurements. V_F means a forward bias voltage, which is applied to the direction from an ITO electrode to an LiF/Al or Al electrode. I_F denotes the current when V_F is applied. Mn^{2+}:MgO powder is an inner standard sample for simultaneous measurements of ESR and EDMR, which is loaded into a quartz capillary tube with 2 mm diameter and which is fixed to an ESR standard quartz tube.

evaporate the solvent. Then, the extra layer at the electrode region was scraped. Successively, LiF and Al were deposited on the P3HT:$PC_{61}BM$ layer of device A. The Al electrode was deposited on the P3HT:$PC_{61}BM$ layer of device B. Both devices were post-annealed at 110 °C for 10 min on the hot plate. Non-annealed and post-annealed devices were ready in each fabrication lot. The fabricated devices were wired and inserted into ESR sample tubes of quartz. Then, the tubes were sealed using epoxy resin in the glovebox. Hereinafter, we designate device A as "device with LiF" and device B is the "device without LiF."

Current density–voltage (J–V) characteristics of the obtained devices were measured using a source meter (2612A; Keithley Instruments, Inc.). A solar simulator (OTENTOSUN-150BXM; Bunkoukeiki Co. Ltd.) was used as a light source. The intensity was tuned to AM 1.5 G, 100 mWcm^{-2} (1 SUN) for J–V measurement under light irradiation. The EDMR spectra were measured using a previously reported instrument setup.[21] To correct the g-factors of EDMR spectral peak positions, as presented in Fig. 1(b), Mn^{2+}:MgO powder was fixed as an inner standard sample to the ESR quartz tube and was measured simultaneously. Magnetic field and g-factors were corrected using a patented method from the literature.[22] The obtained EDMR signal was converted to current variation (ΔI). A ratio ($\Delta I/I_F$) of ΔI and I_F was regarded as an EDMR intensity, where I_F is the constant forward bias current. As described herein, we designate our EDMR detection method as the "Block Lock-In (BLI)" method. In Appendixes A and B, a basic concept of this method and some experimentally obtained results that allow a correction of EDMR intensity are shown. Highly sensitive ESR spectra were obtained using a conventional instrument (JES-FA200; JEOL Ltd.). All experiments were conducted at room temperature (298 K).

III. RESULTS AND DISCUSSION

This section presents experimentally obtained results elucidating the effects of post-annealing from macroscopic and microscopic perspectives. First, the behavior of current density dependent on a forward bias voltage is discussed in accordance with the respective devices. Second, the relation between observed radicals and SDR current is shown based on ESR and EDMR measurement results. Finally, the SDR current changes, as affected by post-annealing and light irradiation, are discussed.

A. Characteristics of J-V curves by post-annealing

Generally, post-annealing treatment enhances V_{OC} or J_{SC} and plays the role of raising the total PCE.[6–10] Based on experimentally obtained J–V characteristics, this section summarizes the effects of post-annealing treatment and differences of devices with LiF and without LiF.

Figure 2 presents results of J–V measurements of devices with LiF and without LiF under light irradiation. The values of J_{SC} and V_{OC} of devices with LiF are decreased by post-annealing treatment, as presented in Fig. 2(a) (Table I). By contrast, the post-annealing treatment increases V_{OC} and the fill factor (FF) of devices without LiF, as presented in Fig. 2(b) (Table I). In this study, as shown in Fig. 1(a), we adopted asymmetric narrow substrates, which have a comparably large active area (25 mm^2), because it is necessary to obtain enough spin amounts for ESR and EDMR measurements. Although there is room for improving performance of the device with a large active area,[23] such design has a disadvantage that the performance decreases because it is difficult to obtain homogeneous film thickness by spin coating. However, these characteristics that are shown in Fig. 2 well correspond to results reported in the literature:[18,19,24] the post-annealing treatment decreases the J_{SC} of devices with LiF and increases the V_{OC} of devices without LiF. Therefore, it can be considered that this investigation using these devices is useful for clarifying microscopic behavior on device fabrication processing.

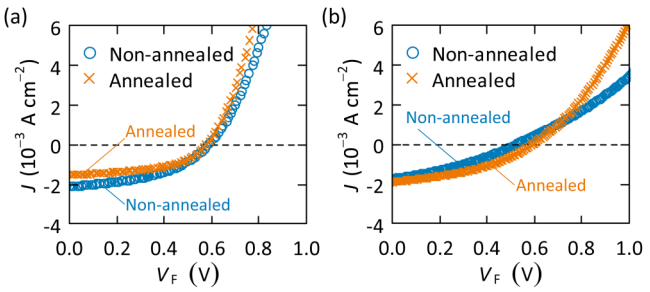

FIG. 2. Results of J–V measurements under light irradiation. (a) J–V characteristics of devices with LiF. Blue open circles show the averaged data for non-annealed devices with LiF. Orange cross markers show averaged data for post-annealed devices with LiF. (b) J–V characteristics of devices without LiF. Blue open circles show averaged data for non-annealed devices without LiF. Orange cross markers show averaged data for post-annealed devices without LiF.

B. Relation between radicals and SDR current by post-annealing

1. Post-annealing effects of devices with LiF

Although earlier reports show that a device with LiF increases $PC_{61}BM$ anion radicals by post-annealing,[19,20] it remains unclear whether the observed radicals contribute to the SDR current or not. This subsection explains post-annealing effects and what radicals are related to SDR current.

Figure 3 shows ESR and EDMR spectra, which reveal effects of the post-annealing treatment to a device with LiF. Figure 3(a) portrays an EDMR spectrum of a non-annealed device. An ESR spectrum of the same device is depicted in Fig. 3(c). The lower spectrum in Fig. 3(a) is a simultaneously obtained ESR spectrum of the Mn^{2+}:MgO powder sample by the BLI method. Using this signal, the magnetic field and the g-factor are corrected. The EDMR spectrum signal intensity was corrected using the following equation:

$$\frac{\Delta I_{(\text{annealed})}}{I_F} = \frac{K^{Mn^{2+}}_{(\text{annealed})}}{K^{Mn^{2+}}_{(\text{non-annealed})}} \times \frac{\Delta I_{(\text{non-annealed})}}{I_F}. \quad (1)$$

In that equation, $\Delta I_{(\text{annealed})}/I_F$ and $\Delta I_{(\text{non-annealed})}/I_F$ are the signal intensities of EDMR of annealed and non-annealed devices.

TABLE I. Performance parameters obtained by *J–V* measurements, spin amounts calculated using ESR measurements, and integral values of the recombination current ratio obtained by EDMR measurements. Error means standard errors $\sigma_{sd}/\sqrt{N}$, where σ_{sd} is the standard deviation. *N* represents the number of experiments.

	LiF/Al electrode (device A)		Al electrode (device B)	
	Non-annealed $N = 6$	Annealed $N = 7$	Non-annealed $N = 5$	Annealed $N = 6$
J_{SC}(mAcm^{-2})	−2.1 ± 0.3	−1.5 ± 0.2	−1.7 ± 0.2	−1.9 ± 0.2
V_{OC} (V)	0.59 ± 0.01	0.58 ± 0.01	0.52 ± 0.02	0.59 ± 0.01
FF	0.45 ± 0.02	0.48 ± 0.02	0.33 ± 0.03	0.39 ± 0.02
PCE (%)	0.56 ± 0.1	0.44 ± 0.09	0.3 ± 0.05	0.44 ± 0.06
$PC_{61}BM^{-}$ N_{spin} (10^{14})	2.7 ± 2	7.0 ± 4	…	…
$P3HT^{+}$ N_{spin} (10^{12})	…	…	3.2 ± 1	2.7 ± 0.6
$PEDOT^{+}$ N_{spin} (10^{14})	1.9 ± 2	1.2 ± 0.8	0.33 ± 0.06	0.33 ± 0.04
Total N_{spin} (10^{14})	4.6 ± 4	8.2 ± 5	0.36 ± 0.05	0.36 ± 0.04
Integral of $\Delta I/I_F$(10^{-4})	2.4 ± 0.7	4.4 ± 1	5.0 ± 1	3.1 ± 0.9

Similarly, $K^{Mn^{2+}}_{(annealed)}$ and $K^{Mn^{2+}}_{(non-annealed)}$ are the respective signal intensities of ESR. An EDMR intensity $\Delta I/I_F$ is the ratio of ΔI because of EDMR and I_F. In all EDMR measurements in Figs. 3 and 4, a forward bias voltage of 0.4 V was applied to devices, which corresponds to almost the maximum voltage of a "bell-shaped curve":[25] characteristic EDMR dependence on the bias voltage. The maximum voltage of a "bell-shaped curve" remains almost unchanged by post-annealing.

The *g*-factor of the peak position of an EDMR spectrum is 2.002. Because a low field shoulder is apparent in this spectrum, this spectrum can be deconvoluted to components of $g = 2.003$ and $g = 2.002$ from fitting analysis as a superposition of two components, which are defined, respectively, as C_b and C_n in Figs. 3(a) and 3(b). Similarly, an ESR spectrum can be regarded as having two components and can be fitted as a superposition of $g = 2.003$ and $g = 2.000$ components, which correspond to C_1 and C_2 in Figs. 3(c) and 3(d). Figures 3(b) and 3(d), respectively, depict EDMR and ESR spectra of the post-annealed device with LiF. As reported by Liu *et al.*,[19,20] a signal of a $PC_{61}BM$ anion radical of $g = 2.000$ is observed. It increases by the post-annealing treatment. Here, the C_2 components (green lines) in Figs. 3(c) and 3(d) correspond to $PC_{61}BM$ anion radicals. However, no signal corresponding to C_2 component was observed in the EDMR spectra of Figs. 3(a) and 3(b). Instead, two components' signals of $g = 2.003$ and $g = 2.002$ were observed. These signals are increased by post-annealing. Generally, an EDMR spectrum comprises two

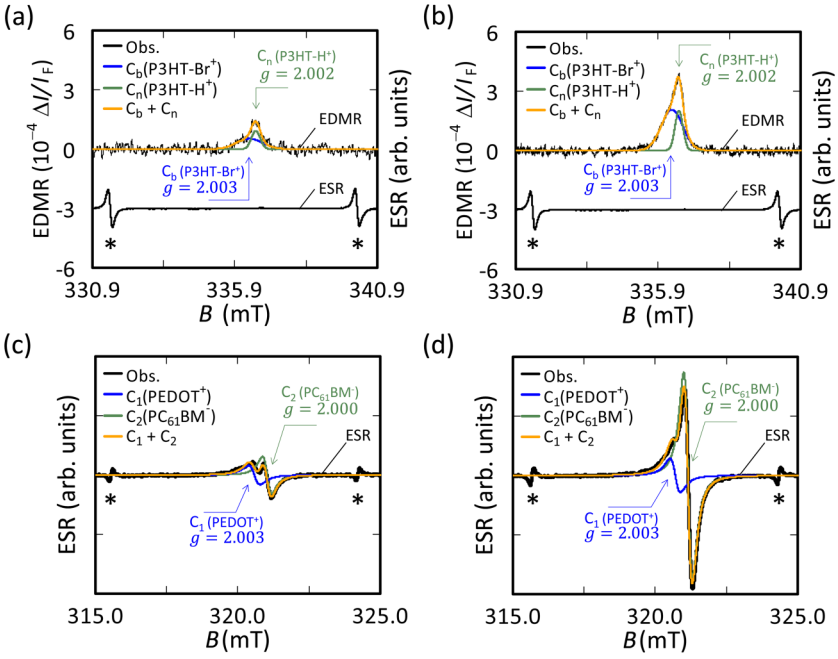

FIG. 3. Comparison of the BLI-detected ESR-EDMR spectra and highly sensitive conventional ESR spectra of devices with LiF. (a) The BLI-detected ESR–EDMR spectra of a non-annealed device with LiF and (b) a post-annealed one. Black solid lines represent observed data. Orange solid lines are fitted by compositions of C_b (blue broad line) and C_n (green narrow line) using a Gaussian function model. (c) An ESR spectrum of a non-annealed device with LiF and (d) a post-annealed one. These two spectra portrayed in (c) and (d) were obtained using a conventional ESR instrument. Black solid lines are observed data. Orange solid lines are fitted by compositions of C_1 (blue line) and C_2 (green line) using a Lorentzian function model. Asterisk marks are peak positions of the Mn^{2+}:MgO inner standard sample. Anti-phase spectra of Mn^{2+}:MgO in (c) and (d) are attributable to the sample-located position in the cavity.

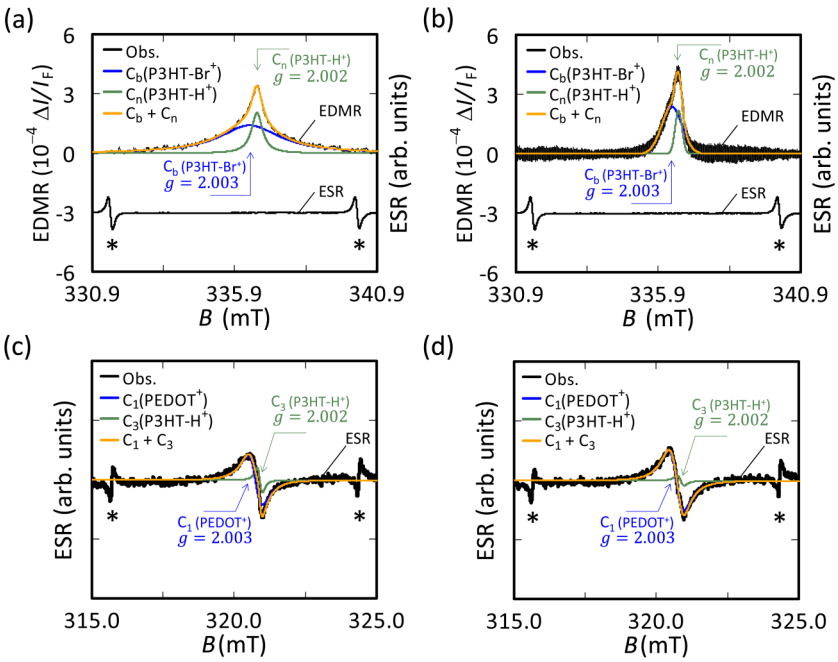

FIG. 4. Comparison of the BLI-detected ESR-EDMR spectra and highly sensitive conventional ESR spectra of devices without LiF. (a) The BLI-detected ESR-EDMR spectra of a non-annealed device without LiF and (b) a post-annealed device without LiF. Black solid lines are observed data. Orange solid lines are fitted by compositions of C_b (blue broad line) and C_n (green narrow line) using Lorentzian (a) and Gaussian (b) function models. (c) An ESR spectrum of a non-annealed device without LiF and (d) a post-annealed device without LiF. These two spectra in (c) and (d) were obtained using the conventional ESR instrument. Black solid lines represent observed data. Orange solid lines are fitted by compositions of C_1 (blue line) and C_3 (green line) using a Lorentzian function model.

components that have the same area intensity if its SDR current is attributable to a spin pair from positive and negative carriers.[26] The observed EDMR spectral components do not have the same area intensities, irrespective of the annealing. Therefore, the observed SDR current for these spectra does not originate from a recombination because of a spin pair, but it can be regarded as indirect recombination currents mediated by two P3HT cation radicals as recombination centers. From an earlier study[27] using P3HT:PC_{61}BM OPVs, Son *et al.* reported that commercially available P3HT materials include P3HT molecules with Br chain ends (P3HT-Br), which could not diminish sufficiently during synthesis. Furthermore, cation radicals on Br ended P3HT have been observed using ESR measurements.[27] Therefore, the observed EDMR spectra can be two indirect recombination currents mediated by two recombination centers of radical cations in P3HT-Br ($g = 2.003$) and P3HT with H chain ends (P3HT-H) ($g = 2.002$) from the assignment of spin species, as found from an earlier study.[27]

A radical component of $g = 2.003$ was also observed from ESR measurements. As discussed later, compared to results obtained for devices without LiF in Fig. 4, the signal intensity and the linewidth remain almost unchanged irrespective of the annealing. Therefore, these two radicals can be regarded as different chemical species. The origin of the C_b component in the EDMR spectrum might be a P3HT-Br cation radical. That of the C_1 component in an ESR spectrum might be a PEDOT cation radical.[28] New findings obtained using ESR and EDMR measurements together indicate that PC_{61}BM anion radicals increased by post-annealing do not contribute directly to SDR current and indicate that the indirect recombination current mediated by two related P3HT cation radicals increases.

This report is the first to describe a study of the application of the BLI method to organic semiconductor devices. Nevertheless, it was unfortunately impossible to obtain sufficient sensitive ESR spectra that can be discussed quantitatively. Some room remains to improve instrumental sensitivity. Although it is not sufficient spectral quality, ESR and EDMR components of a device can be observed simultaneously by raising the amplifier gain and by accumulating data. As a demonstration, measurement examples using the BLI method are presented in Fig. 9. It is noteworthy that distinguishing ESR from EDMR under *in situ* conditions was accomplished. Conventional measurements of ESR and EDMR were unable to achieve this observation.

2. Post-annealing effects of devices without LiF

To ascertain whether the increase of the SDR current on devices with LiF is attributable to the LiF layer or not, the post-annealing effects of devices without LiF were investigated. This subsection presents similar ESR-EDMR data for devices with LiF and assesses a relation between cation radicals and the SDR current.

Post-annealing effects of a device without LiF are portrayed in Fig. 4. The EDMR spectral components of devices without LiF are the same as those of devices with LiF, which consisted of C_b ($g = 2.003$) and C_n ($g = 2.002$) components. Similarly, the area intensities of C_b and C_n spectral regions are not the same. However, it is noteworthy that the spectral linewidths of C_b and C_n in Fig. 4(a) are, respectively, very broad ($H_{1/2}(C_b) = 2.6$ mT, $H_{1/2}(C_n) = 0.5$ mT, where $H_{1/2}$ denotes the full width at half maximum (FWHM)). Additionally, they have Lorentzian line shapes. By post-annealing of this device, as portrayed in Fig. 4(b), spectral line shapes of EDMR change to Gaussian, as observed for

devices with LiF. Also, the integral strength of the spectrum diminishes. Linewidths of C_b and C_n components, respectively, sharpen to become $H_{1/2}(C_b) = 0.8$ mT and $H_{1/2}(C_n) = 0.3$ mT. That sharpening indicates that total indirect recombination current decreases because of the post-annealing treatment. In contrast to the case of devices with LiF, the ESR spectra have no $PC_{61}BM$ component ($g = 2.000$), as shown in Figs. 4(c) and 4(d). The main component of the ESR spectra is attributable to PEDOT cation radicals of C_1 ($g = 2.003$). In fact, a tiny amount of P3HT-H cation radicals of C_3 ($g = 2.002$) can also be observed. Regardless of the post-annealing, the line width of the C_1 component does not change [$H_{1/2}(C_1) = 0.9$ mT]. Additionally, the total area intensities of the ESR spectra are almost identical. This similarity implies that the change of the indirect recombination current in this case is not attributable to variation of the radical amounts.

Table I presents obtained data. As shown in the "LiF/Al electrode" columns, the device with LiF shows decreased J_{SC} and PCE by post-annealing. At the same time, $PC_{61}BM$ anion radicals and the total SDR current ratio mediated by P3HT cation radical centers increase. By contrast, as shown in the "Al electrode" columns, the device without LiF increases V_{OC} and PCE by the post-annealing treatment. Although radical amounts ($P3HT^+$ N_{spin}, $PEDOT^+$ N_{spin}, Total N_{spin}) observed in the device without LiF do not change considerably, the total amount of the indirect recombination current mediated by P3HT cation radical centers (integral of $\Delta I/I_F$) decreases. A characteristic point is to change the line shapes of EDMR spectra from Lorentzian to Gaussian by the post-annealing treatment.

C. Changes of SDR current affected by Al electrode structures and light irradiation

Based on the results described above, the relation between the variation of the electrode interface by the post-annealing treatment and the SDR current can be discussed as follows.

First, post-annealing effects of the devices with LiF are discussed. With non-annealing, as presented in Fig. 5(a), the interface at an active layer that includes P3HT and the Al electrode is protected by a very thin LiF layer. As a result, an LiF layer plays a role as an effective HBL, which inhibits the hopping transfer of positive charges from a positive polaron of $P3HT^+$ radicals. At the same time, this HBL inhibits generating the exclusive spin pair of an electron in an Al electrode and a hole in $P3HT^+$. In such a case, ESR transition of spins in the highest occupied molecular orbital (HOMO) of $P3HT^+$ cannot promote to generate the spin singlet state by accepting electrons in the Al electrode. Therefore, it is difficult to flow the SDR current. However, by the post-annealing treatment, a LiF layer resolves; Li atoms diffuse into an organic active layer.[18] Furthermore, an LiF/Al electrode chemically reacts to an organic compound and generates a charge transferred complex or an organic anion.[29–31] Concretely, the chemical reaction, as shown in Eq. (2), forms $PC_{61}BM$ anion radicals,

$$3LiF + Al + 3PC_{61}BM- > AlF_3 + 3Li^+PC_{61}BM^-. \quad (2)$$

This can be considered to show that the formed anion radicals induce the scattering of electric charges at the interface and consequently decrease the current flow.[19,20] The present study shows that post-annealing not only forms $PC_{61}BM$ anion radicals, but it also increases the indirect recombination current mediated by P3HT cation radical centers. The reason can be considered that the interface, which is partially destroyed by the chemical reaction of Eq. (2), enlarges the contact cross section between Al that donates electrons and P3HT cations that supply holes [Fig. 5(a)]. Such an HBL destruction makes it easy to pair an electron in an Al electrode and a hole of $P3HT^+$ exclusively as shown in Fig. 5(a). ESR transitions of spins in $P3HT^+$ can change the population balance of a spin singlet state and a triplet state. Therefore, EDMR spectra can be obtained because the variation of spin singlet population changes the SDR current. At this time, the HOMO level of $P3HT^+$ plays a role as a relay point and promotes to recombine with other holes that are supplied from ITO. This means the indirect SDR current where $P3HT^+$ is a recombination center. Consequently, an LiF/Al layer loses HBL ability. Also, the indirect recombination rate would be enhanced. Comparison of ESR to EDMR clarifies that $PC_{61}BM$ anion radicals do not contribute to the SDR current.

Second, post-annealing effects of devices without LiF are discussed hereinafter. An Al electrode of a device without LiF has no HBL as a LiF device does. Therefore, the variation of an interface by post-annealing treatment differs from that of a device with an LiF/Al electrode. Reportedly, the organic active layer consisting of P3HT and $PC_{61}BM$ segregates P3HT polymer molecules upward to the surface of the BHJ layers because of the surface energy when BHJ layers are formed. Also, by post-annealing, $PC_{61}BM$ with high surface energy diffuses and forms an intermediate layer at the interface of an Al electrode that has similarly high surface energy.[24] As a result, the total surface energy is stabilized. This intermediate layer is inserted between Al and P3HT, where it serves in the role as an HBL. Under a non-annealed condition, as presented in Fig. 5(b), because of the segregation of P3HT on an Al electrode, the volume of P3HT facing an Al electrode is large. Therefore, P3HT cation radicals, as positive polarons, might be in an easily mobile environment, which would engender increased dipole–dipole interaction among radicals. Such spin–spin interaction broadens the spectral linewidth and also makes its line shape Lorentzian by enhancing magnetic homogeneity. At the same time, similarly to the post-annealed device with LiF, exclusive spin pairs increase because of the lack of HBL as shown in Fig. 5(b). Therefore, the SDR current can flow easily. Because the post-annealing treatment forms an interlayer of $PC_{61}BM$ between Al and P3HT and becomes an HBL, the characteristics of J–V presented in Fig. 2(b) are improved. The resolution of the segregation and the mixing of P3HT and $PC_{61}BM$ by the post-annealing treatments weaken the polarons mobility and decrease the contact probability. This situation is similar to that of a trapped state of P3HT cation radicals. Furthermore, a decreased probability of contacts between P3HT and Al can be expected to diminish the recombination current. An indirect recombination current mediated by trapped paramagnetic electrons is generally explained by the Shockley–Hall–Read model.[35] When capture cross sections of holes and electrons are presumed to be the same, the indirect

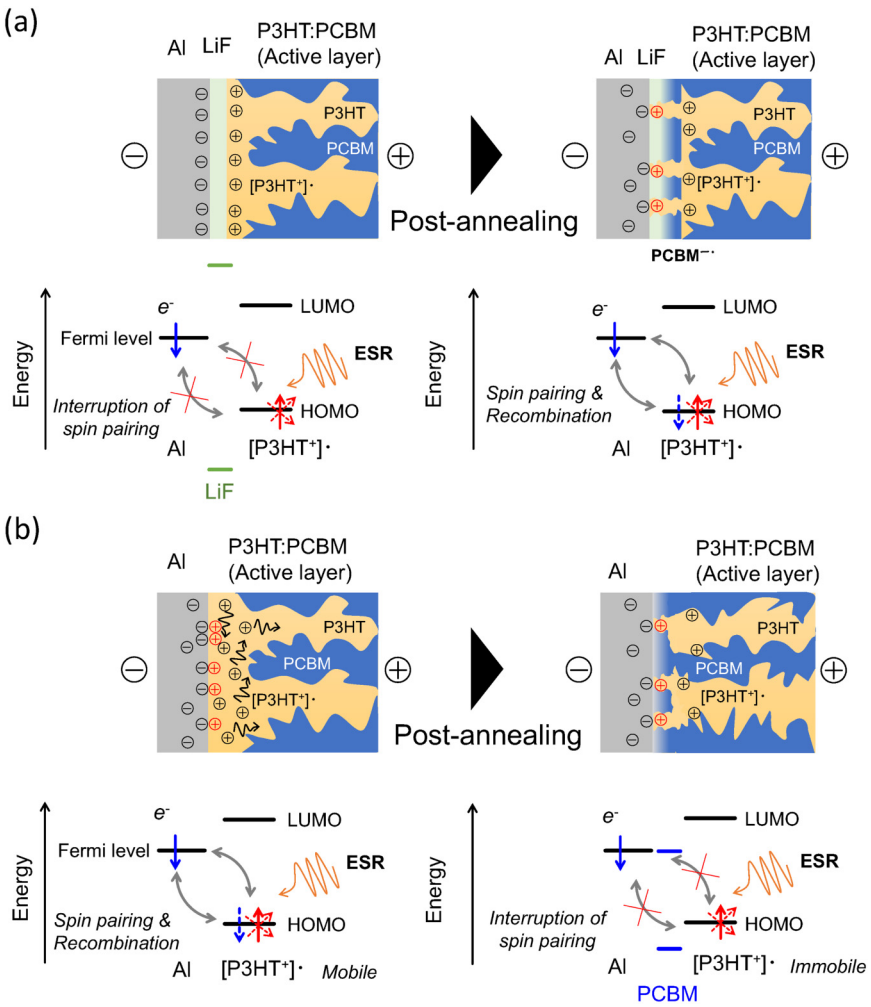

FIG. 5. Schematic drawings of changes of an interface structure by the post-annealing process and the energy levels between the Al electrode and the positive polaron ($P3HT^+$ radical) for the cases of (a) the devices with LiF and (b) the devices without LiF. The red symbol of ⊕ denotes a P3HT cation radical, which is a recombination center. Symbols of ⊖ signify electrons. Horizontal bars show the energy levels. A bar at Al denotes the Fermi level. Upper and lower bars of LiF, respectively, stand for the conduction band minimum (CBM) and the valence band maximum (VBM). The other bars, respectively, denote the highest occupied molecular orbital (HOMO) and the lowest occupied molecular orbital (LUMO) of P3HT or $PC_{61}BM$. The relative positions of the bars are shown based on the literature.[32–34] Red dashed arrows indicate the ESR transitions.

recombination rate U mediated by defects is expressed as[35]

$$U = \sigma v_{TH} N_t \frac{pn - n_i^2}{n + p + 2n_i \cosh \frac{E_t - E_i}{k_B T}}, \tag{3}$$

where σ stands for a capture cross section, v_{TH} denotes the thermal velocity of an electron, N_t expresses the concentration of recombination centers, p and n are, respectively, stand for the densities of holes and electrons, n_i signifies the intrinsic carrier density, E_t is the energy level of a recombination center, E_i symbolizes the Fermi energy, k_B is Boltzmann's constant, and T is the absolute temperature. In this case, by regarding the amounts of the recombination center (P3HT cation radicals), the forward bias, and the injected carrier density being constant, the variation of EDMR signal intensities can be regarded as a variation of a capture cross section, as Eq. (3) shows: it can be inferred that post-annealing of a device without LiF generates a new interlayer of $PC_{61}BM$ on the Al electrode and decreases the capture cross sections of P3HT. Therefore, it leads to diminished SDR current mediated by P3HT cation radicals.

Indirect spin-dependent current can be regarded as leakage current, because its current direction is opposite to J_{SC}. In addition, the electromotive force corresponding to V_{OC} induced by light irradiation can be expected to weaken by the indirect spin-dependent current. Therefore, it might be considered that a change of SDR current correlates to an effect of macroscopic performances of OPVs.

Finally, the relation between the variation of SDR current and solar-cell performance is considered. Figure 6 presents a comparison of EDMR spectra of a device with LiF under dark and UV-irradiated conditions. The findings indicate that the SDR current is increased significantly by UV-irradiation. This rate of enhancement is dependent on the irradiation power. We are now planning to conduct some experiments to elucidate the irradiation effects, which will be undertaken in future work. As described above, the SDR current under a forward biased condition can also be regarded as the leakage current under light irradiation of solar

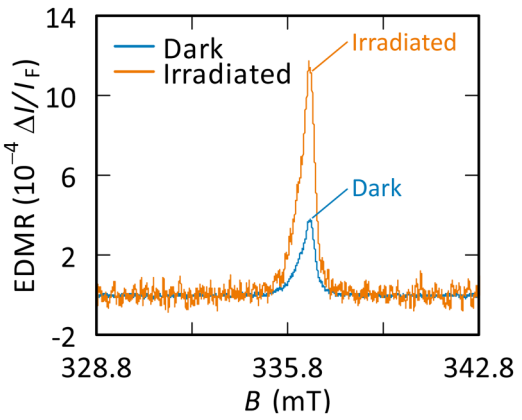

FIG. 6. Light irradiation effects of a device with LiF (post-annealed one). The blue solid line is an EDMR spectrum under dark condition. The orange solid line is a UV-irradiated one using a spot light source (LIGHTNINGCURE®LC8; Hamamatsu Photonics K.K.). The irradiated power is 1.8 mWcm^{-2} at 440 nm. V_F of 0.57 V was applied in both measurements.

cells because its current direction is opposite to the light-induced current. Not only a change of interface structure of an electrode but also an increase of leakage current attributable to light irradiation would be disadvantageous for improving and maintaining the OPV performances. Therefore, regulation of the electrode interface and the capture cross sections of polarons are important difficulties to be overcome for the improvement of OPVs.

IV. CONCLUSION

This study investigated the correlation between post-annealing treatment and SDR current using OPVs consisting of a P3HT: $PC_{61}BM$ blended active layer and two kind electrode structures of LiF/Al and Al. It has been known conventionally that post-annealing generates a chemical reaction at the Al electrode interface and that it forms $PC_{61}BM$ anion radicals leading to electric charge scattering. As a further approach, after applying an originally developed simultaneous detection method of ESR and EDMR spectra to the OPVs for the first time ever reported, we found that indirect SDR current mediated by P3HT cation radical centers increased by post-annealing of the device with an LiF/Al electrode, although it decreased in the case of the device with an Al single electrode. The combined use of ESR and EDMR measurements can distinguish the roles of $PC_{61}BM$ radicals and P3HT ones and can elucidate the relation between changes of the amounts of radical species and SDR current. The EDMR spectral line shape of the device without LiF changes drastically from Lorentzian to Gaussian by post-annealing. Based on the non-susceptible property of P3HT cation radicals to annealing and the structural change occurring at the interface between Al and P3HT, it can be inferred that the change of the capture cross sections of P3HT caused by the change of the contact area at the interface affects the indirect SDR current. The SDR current under the forward bias might be leakage current against the light-induced current of solar cells under irradiation. In fact, the EDMR signal intensity of a device with LiF under irradiation was enhanced compared to a dark condition. These findings might be useful information to achieve additional improvements of OPVs.

ACKNOWLEDGMENTS

The author would like to thank Mr. A. Sato for advice related to sample fabrication and useful discussion. This work was partially supported by JST MIRAI, Japan (Grant Nos. JPMJMI20C5, JPMJMI22C1, and JPMJMI22E2) and by NEDO Green Innovation, Japan.

AUTHOR DECLARATIONS

Conflict of Interest

Takayuki Suzuki has patent JP7114406B2.

Author Contributions

Takayuki Suzuki: Conceptualization (equal); Formal analysis (lead); Investigation (lead); Methodology (lead); Visualization (lead); Writing – original draft (equal). **Kazuhiro Marumoto:** Conceptualization (equal); Formal analysis (equal); Funding acquisition (lead); Supervision (lead); Writing – review & editing (equal).

DATA AVAILABILITY

The data that support the findings of this study are available from the corresponding author upon reasonable request.

APPENDIX A: MEASUREMENT METHOD AND ITS UTILITY

Here, we briefly present a concept of ESR–EDMR simultaneous detection used for this study, as shown in Fig. 7. Detailed information has been presented in the relevant literature.[21] This method, which measures continuous (cw)-ESR and cw-EDMR spectra simultaneously in one scan, divides a period of microwave ON/OFF modulation to two blocks, which consist of the former and latter regions. The former is assigned for microwave amplitude modulation. The latter is for magnetic field modulation. Applying the respective modulations alternately and then doing phase-sensitive detection by synchronized reference signals to individual modulation frequencies, the ESR and EDMR spectra are obtainable under their respectively optimized conditions. As described in the main text, this method is designated as the "block lock-in (BLI)" method.

As presented in Fig. 7(a), in the former period (Block 1) of T_{ω_1}, the power level of the microwave power is modulated with a frequency of $\omega_1/2\pi$. The pulse height level used for this study is 60 mW; also, the 1 mW offset level is kept in the power-off period. This offset power is optimized for measuring the ESR spectra. In the latter period (Block 2) of T_{ω_1}, a static magnetic field is modulated with a frequency of $\omega_2/2\pi$ using modulation coils in the cavity. This amplitude strength corresponds to a magnetic modulation width, which is set to 0.1 mT for this study. Two modulation signals are alternately applied during the periods of Block 1 and

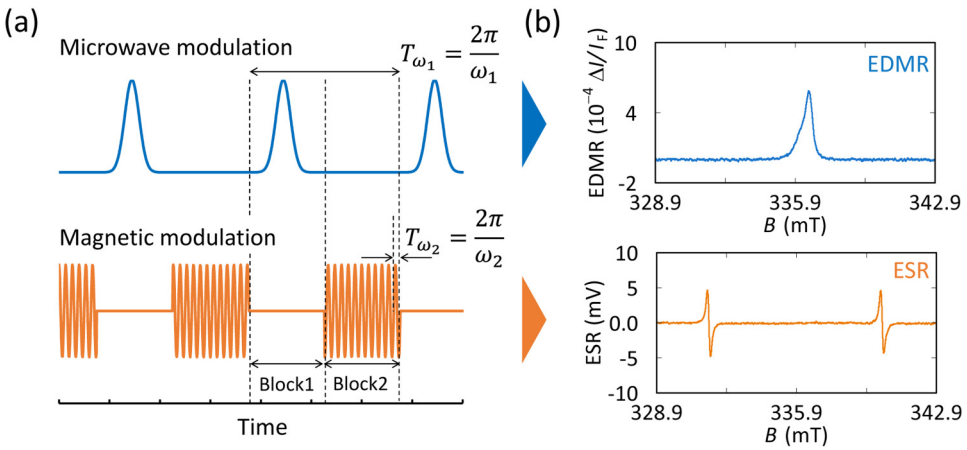

FIG. 7. Simultaneous detection scheme used for this study. (a) Modulation signals for the simultaneous detection of ESR–EDMR. Upper Gaussian pulses are to modulate the microwave to obtain the EDMR signals, where the modulation frequency is $\omega_1 = 2\pi f_1$ and where the period is $T_{\omega_1} = 2\pi/\omega_1$. Lower sinusoidal pulses are used to modulate the magnetic field to obtain the ESR signals, where modulation frequency is $\omega_2 = 2\pi f_2$ and its period is $T_{\omega_2} = 2\pi/\omega_2$. (b) Simultaneously obtained individual spectra of EDMR (upper) and ESR (lower). These spectra are obtained using the lock-in detection using the respective reference frequency of $\omega_1/2\pi$ and $\omega_2/2\pi$.

Block 2 with a sweeping static magnetic field. Using two lock-in amplifiers, two different modulated signals are individually lock-in detected by the reference signals synchronized to the frequencies of $\omega_1/2\pi$ and $\omega_2/2\pi$. Therefore, the EDMR and ESR spectra can be obtained simultaneously under their respectively optimized conditions, as shown in Fig. 7(b). The set frequencies are, respectively, $\omega_1/2\pi = 70$ Hz and $\omega_2/2\pi = 100$ kHz.

The ESR signals are dependent on changes of the Q_L values and the B_1 strength of a cavity resonator, where changes are caused by differences of each device's quality and position in the cavity. Similarly, the EDMR signals vary because of the Q_L values and B_1 strength. If the dependence is the same, then the BLI method can correct the variation of EDMR signals by ESR signal intensities obtained simultaneously. This method is based on the following BLI experimentally obtained results.

Figure 8 presents experimentally obtained results for the dependence of ESR and EDMR signals on the Q_L values of a cavity and the power dependence of the EDMR signal. The measured samples are Mn^{2+}:MgO powder for ESR and a device with LiF for EDMR. The cw-ESR signals are well-known to be proportional to the Q_L values of the microwave cavity.[36] As shown in Fig. 8(a), both the ESR and EDMR intensities are proportional to the Q_L values. Figure 8(b) shows the microwave power (P) dependence of EDMR intensities. Up to around $P = 60$ mW ($\sqrt{P} = 7.75$) used for this study, the EDMR signals are proportional to the square root of power. In general, the EDMR signals show different microwave power dependence in accordance with power levels.[37–39] The power level of 60 mW is associated with a strong power-dependent condition, because EDMR signals are proportional to the square root of the microwave power. One can reasonably infer that ESR and EDMR have the same power-dependent property: B_1 strength dependence. Therefore, it is expected that EDMR signals of different devices can be compared correctly by a ratio of ESR signal intensities obtained simultaneously. Such a quantitative comparison of EDMR signals would be impossible using the conventional EDMR measurement method.

APPENDIX B: ESR AND EDMR SPECTRA OF DEVICES WITH LIF OBTAINED SIMULTANEOUSLY USING THE BLI METHOD

This study applied the BLI method to OPVs for the first time ever reported. Unfortunately, because the instrumental sensitivity of the ESR measurement circuit remains insufficient, we used this method only for the correction of g factors and EDMR intensities. In this appendix, we have presented demonstration data of real simultaneous detection of ESR and EDMR spectra obtained by raising the amplifier gain and long-term accumulation. As shown

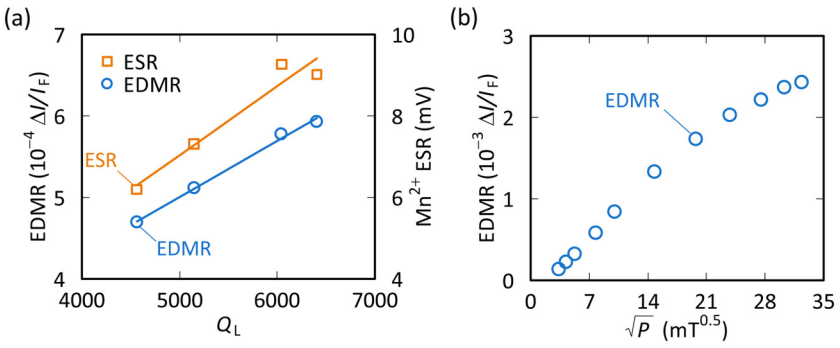

FIG. 8. (a) ESR and EDMR intensities that depend on Q_L values of a microwave cavity using a BLI method. Q_L values are controlled by taping numbers of Scotch® tape pieces. Measured samples are Mn^{2+}:MgO powder for ESR and a device with LiF for EDMR as presented in Fig. 1(a). (b) Incident microwave power (P) dependence of the EDMR signal intensity using a device with LiF.

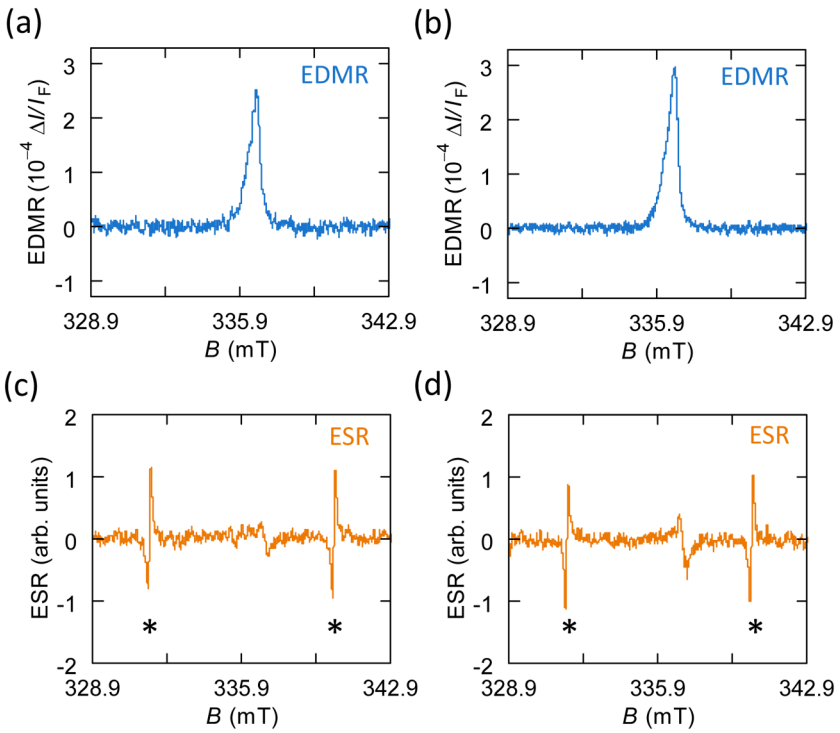

FIG. 9. Comparison of the BLI-detected ESR-EDMR spectra of devices with LiF. (a) Simultaneously obtained EDMR spectrum of a device with LiF (non-annealed one). (b) Similarly obtained EDMR spectrum of a device with LiF (annealed one). (c) An ESR spectrum obtained simultaneously with the EDMR spectrum of (a). (d) An ESR spectrum obtained simultaneously with the EDMR spectrum of (b). Asterisk marks are peak positions of an Mn^{2+}:MgO inner standard sample. The microwave power is 4 mW for ESR measurements and is 60 mW for EDMR measurements. For EDMR detection, a lock-in amplifier (5600A; NF Corp.) was used, with sensitivity set to 1.0 V, time constant set to 30 ms, and the dynamic reserve set as "low." For ESR detection, a lock-in amplifier (LI5655; NF Corp.) was used, with sensitivity set to 2.0 mV, time constant set to 20 ms, and the dynamic reserve set as "high." The sweep time was set to 30 s. The number of spectral accumulations was 196. V_F of 0.47 V was applied in both measurements.

in Fig. 9, it can be ensured that the ESR signal ($PC_{61}BM$ anion radicals) and the EDMR signal (P3HT cation radicals) are increased by post-annealing treatment. We are now striving to improve its sensitivity for future applications.

REFERENCES

[1]C. W. Tang, Appl. Phys. Lett. **48**, 183 (1986).
[2]L. Ding, *Organic Solar Cells: Materials Design, Technology and Commercialization* (Wiley, 2022).
[3]K. Jin, Z. Xiao, and L. Ding, J. Semicond. **42**, 060502 (2021).
[4]W. Gao *et al.*, Adv. Mater. **34**, 2202089 (2022).
[5]See https://www.nrel.gov/pv/cell-efficiency.html for "Best Research-Cell Efficiency Chart."
[6]F. Padinger, R. Rittberger, and N. Sariciftci, Adv. Funct. Mater. **13**, 85 (2003).
[7]W. Ma, C. Yang, X. Gong, K. Lee, and A. J. Heeger, Adv. Funct. Mater. **15**, 1617 (2005).
[8]X. Liu *et al.*, Mater. Chem. Front. **1**, 2057 (2017).
[9]L. Zhu *et al.*, Adv. Energy Mater. **10**, 1904234 (2020).
[10]W. Zhu *et al.*, J. Am. Chem. Soc. **142**, 14532 (2020).
[11]A. Hayakawa, O. Yoshikawa, T. Fujieda, K. Uehara, and S. Yoshikawa, Appl. Phys. Lett. **90**, 163517 (2007).
[12]A. K. K. Kyaw *et al.*, ACS Nano **7**, 4569 (2013).
[13]L. S. Hung, C. W. Tang, and M. G. Mason, Appl. Phys. Lett. **70**, 152 (1997).
[14]G. E. Jabbour *et al.*, Appl. Phys. Lett. **71**, 1762 (1997).
[15]S. E. Shaheen *et al.*, J. Appl. Phys. **84**, 2324 (1998).
[16]C. J. Brabec, S. E. Shaheen, C. Winder, N. S. Sariciftci, and P. Denk, Appl. Phys. Lett. **80**, 1288 (2002).
[17]F. Wen, W. Li, Z. Liu, and H. Wei, Mater. Chem. Phys. **95**, 94 (2006).
[18]F. Li, J. Zhao, K. Yao, and Y. Chen, Chem. Phys. Lett. **553**, 36 (2012).
[19]D. Liu *et al.*, Appl. Phys. Lett. **104**, 243903 (2014).
[20]K. Marumoto, D. Liu, and M. Yabusaki, J. Photopolym. Sci. Technol. **29**, 541 (2016).
[21]T. Suzuki, Rev. Sci. Instrum. **90**, 073102 (2019).
[22]Y. Mizuta, "Electron spin resonance spectroscopy," US patent 4,994,745 (19 February 1991).
[23]D. Chalal, R. Garuz, D. Benachour, J. Bouclé, and B. Ratier, Synth. Met. **212**, 161 (2016).
[24]A. Orimo *et al.*, Appl. Phys. Lett. **96**, 043305 (2010).
[25]Y. Kamigaki, T. Miyazaki, N. Yoshihiro, K. Watanabe, and K. Yokogawa, J. Appl. Phys. **84**, 2193 (1998).
[26]H. Morishita *et al.*, Phys. Rev. B **89**, 125311 (2014).
[27]D. Son, T. Kuwabara, K. Takahashi, and K. Marumoto, Appl. Phys. Lett. **109**, 133301 (2016).
[28]K. Marumoto, T. Fujimori, M. Ito, and T. Mori, Adv. Energy Mater. **2**, 591 (2012).
[29]M. G. Mason *et al.*, J. Appl. Phys. **89**, 2756 (2001).
[30]C.-I. Wu, G.-R. Lee, and T.-W. Pi, Appl. Phys. Lett. **87**, 212108 (2005).
[31]D. Son, Y. Shimoi, and K. Marumoto, Mol. Cryst. Liq. Cryst. **599**, 153 (2014).
[32]Y. Li, H. Chen, and J. Zhang, Nanomaterials **11**, 1404 (2021).
[33]X. Wang *et al.*, Chin. J. Polym. Sci. **39**, 831 (2021).
[34]V. Singh, A. K. Thakur, S. S. Pandey, W. Takashima, and K. Kaneto, Org. Electron. **9**, 790 (2008).
[35]S. Sze, Y. Li, and K. Ng, *Physics of Semiconductor Devices*, 4th ed. (Wiley, 2021), pp. 37–43.
[36]C. Poole, "Electron spin resonance: A comprehensive treatise on experimental techniques," in *Dover Books on Physics* (Dover Publications, 1996).
[37]Z. Xiong and D. J. Miller, Appl. Phys. Lett. **63**, 352 (1993).
[38]K. Lips, C. Lerner, and W. Fuhs, J. Non-Cryst. Solids **198–200**, 267 (1996).
[39]G. Kawachi, C. F. O. Graeff, M. S. Brandt, and M. Stutzmann, Jpn. J. Appl. Phys. **36**, 121 (1997).